Acta Mechanica 113, 185–203 (1995)

ACTA MECHANICA

Effect of loading direction and initial imperfections on the development of dynamic shear bands in a FCC single crystal

R. C. Batra, Blacksburg, Virginia, and **Z. G. Zhu,** Troy, Michigan

(Received September 27, 1993; revised April 19, 1994)

Summary. We study plane strain dynamic thermomechanical deformations of a FCC single crystal deformed at an average strain-rate of 1 000 s^{-1} along the crystallographic direction [380] with the plane of deformation parallel to the plane (001) of the single crystal. Four different situations are studied; in the first two there is no initial imperfection assumed in the crystal and it is either compressed or pulled, and in the other two the crystal is compressed but either the initial temperature is nonuniform or a small region around the centroid of the cross-section is misoriented relative to the rest of the cross-section. In each case, all twelve slip systems are assumed to be potentially active, and the crystal material is presumed to exhibit strain hardening, strain-rate hardening, and thermal softening. These effects are modelled by using a simple combined isotropic-kinematic hardening expression for the critical resolved shear stress, proposed by Weng, and modified to incorporate the effect of thermal softening of the material. It is found that each one of the slip systems $(111)[\bar{1}10]$, $(11\bar{1})[\bar{1}10]$, $(\bar{1}11)[110]$, and $(\bar{1}1\bar{1})[110]$ contributes essentially equally to the plastic deformations of the crystal and these slip systems become active soon after the load is applied. The same holds for the slip systems $(111)[01\bar{1}]$, $(11\bar{1})[011]$, $(\bar{1}11)[101]$, and $(1\bar{1}1)[\bar{1}01]$ except that they are active in a region different from that of the previous one. The remaining four slip systems either stay inactive throughout the deformation process, or become active at late stages of the deformation.

1 Introduction

Shear bands, i.e., regions of localized shearing, in FCC single crystals deformed quasistatically have been observed by several investigators (e.g. see Sawkill and Honeycombe [1], Price and Kelly [2], Saimoto et al. [3], Chang and Asaro [4]). Zikry and Nemat-Nasser [5] and Zhu and Batra [6] have analyzed numerically dynamic shear bands in a FCC single crystal deformed in plane strain tension and compression respectively. Whereas Zikry and Nemat-Nasser employed the double cross-slip model due to Koehler [7] and Orowan [8] during the entire loading history, Zhu and Batra assumed that all twelve slip systems are potentially active. We refer the reader to the paper by Zikry and Nemat-Nasser for additional references on the subject, and a discussion of the earlier work. Here we assume that all twelve slip systems are potentially active, the crystal is deformed along the crystallographic direction [380] with its deformation in a plane parallel to the plane (001) of the single crystal, and consider four different situations outlined in the abstract above. The consideration of all twelve slip systems will enable us to consider fully the geometric softening associated with the rotation of slip planes to more favorable orientations. The reason for selecting this loading configuration is that it causes a large asymmetry in the orientation of slip systems and hence eliminates the need to introduce any artifical defect that will serve as a nucleation site for the shear band. A comparison of results for compression and tension loading should enable us to delineate which type of loading induces more geometric softening. Also results computed with a defect introduced at the block centroid will reveal if the effects of geometric softening are enhanced or inhibited by the presence of a defect.

The shapes and locations of the shear bands and the rotation of the crystal lattice within the severely deformed region are different in each case. Thus, the loading direction i.e. tension or compression and the type of material imperfection i.e. nonuniform initial temperature or misorientation of the lattice structure influence strongly the locations, orientations and the form of shear bands.

2 Formulation of the problem

We employ a set of fixed rectangular Cartesian coordinates to describe deformations of a FCC single crystal of square cross-section of sides 2H, deformed along the crystallographic direction [380], and the $x_1 - x_2$ plane of deformation parallel to the plane (001) of the single crystal. Thus, the angle between the loading direction and the principal axis of the single crystal equals 20°. In Eulerian description, the balance of mass, balance of linear momentum and the balance of internal energy are

$$\dot{\varrho} + \varrho v_{i,i} = 0, \tag{1}$$

$$\varrho \dot{v}_i = \sigma_{ij,j}, \tag{2}$$

$$\varrho c \dot{\theta} = k\theta_{,ii} + \sigma_{ij} D_{ij}^p, \tag{3}$$

where ϱ is the present mass density, v_i the velocity of a material particle, a superimposed dot indicates the material time derivative, a comma followed by an index j denotes partial derivative with respect to the present position x_j of a material point, a repeated index implies summation over the range of the index, σ_{ij} is the Cauchy stress tensor, c the specific heat, k the thermal conductivity, and D_{ij}^p is the plastic part of the strain-rate tensor D_{ij} defined by

$$D_{ij} = \frac{1}{2}(v_{i,j} + v_{j,i}). \tag{4}$$

In Eq. (3) we have assumed that Fourier's law of heat conduction holds, and all of the plastic working is converted into heating. This is not strictly valid for a material that exhibits substantial amount of kinematic hardening for which a considerable amount of plastic working will be stored as irrecoverable energy. Also, for polycrystalline materials Farren and Taylor [9] and Sulijoadikusumo and Dillon [10] have reported that only 90−95% of plastic working is converted into heating. Here the assumption that all of plastic working is converted into heating is made for the sake of simplicity. Since in plane strain deformations $D_{33}^p$and σ_{33} need not equal zero, the indices i and j in the last term on the right-hand side of Eq. (3) range over 1, 2, and 3. We assume that the strain-rate tensor D_{ij} given by (3) and the spin tensor W_{ij} defined by

$$W_{ij} = \frac{1}{2}(v_{i,j} - v_{j,i}) \tag{5}$$

have additive decompositions into elastic and plastic parts, i.e.

$$\boldsymbol{D} = \boldsymbol{D}^e + \boldsymbol{D}^p, \qquad \boldsymbol{W} = \boldsymbol{W}^e + \boldsymbol{W}^p. \tag{6}$$

The plastic parts $\boldsymbol{D}^p$ and $\boldsymbol{W}^p$ are determined by the local plastic slip rates of all active slip systems at a material point, and are given by

$$D_{ij}^p = \sum_\alpha \overset{(\alpha)}{v}_{ij} \overset{(\alpha)}{\dot{\gamma}}{}^p, \qquad W_{ij}^p = \sum_\alpha \overset{(\alpha)}{\omega}_{ij} \overset{(\alpha)}{\dot{\gamma}}{}^p, \tag{7}$$

where $\overset{(\alpha)}{\dot{\gamma}}{}^p$ is the plastic strain-rate of the α^{th} slip system, and

$$\overset{(\alpha)}{v}_{ij} = \frac{1}{2}(\overset{(\alpha)}{b}_i \overset{(\alpha)}{n}_j + \overset{(\alpha)}{b}_j \overset{(\alpha)}{n}_i), \qquad \overset{(\alpha)}{\omega}_{ij} = \frac{1}{2}(\overset{(\alpha)}{b}_i \overset{(\alpha)}{n}_j - \overset{(\alpha)}{b}_j \overset{(\alpha)}{n}_i), \tag{8}$$

$\boldsymbol{b}$ is a unit vector in the slip direction and $\boldsymbol{n}$ a unit vector normal to the slip plane. Vectors $\boldsymbol{b}$ and $\boldsymbol{n}$ are assumed to rotate with the elastic spin of the lattice, and their rates of change are given by

$$\dot{b}_i = W_{ij}^e b_j, \qquad \dot{n}_i = W_{ij}^e n_j. \tag{9}$$

Henceforth, we assume that elastic strains everywhere remain infinitesimal and are negligible as compared to the plastic strains. During plane strain deformations of the crystal, the rotation of a slip system can be characterized by the angle change ϕ of the projective direction of the slip vector in the $x_1 - x_2$ plane, and given by

$$\dot{\phi} = W_{21}^e = W_{21} - \sum_\alpha \overset{(\alpha)}{\omega}_{21} \overset{(\alpha)}{\dot{\gamma}}{}^p. \tag{10}$$

We assume that the material properties of the single crystal are strain-rate dependent, and the plastic slip rate of the α^{th} slip system is related to the resolved shear stress on it by the power law:

$$\overset{(\alpha)}{\dot{\gamma}}{}^p = \begin{cases} \overset{(\alpha)}{\dot{\gamma}}_0 \dfrac{\overset{(\alpha)}{\tau}}{\overset{(\alpha)}{\tau}_c} \left(\dfrac{|\overset{(\alpha)}{\tau}|}{\overset{(\alpha)}{\tau}_c} \right)^{1/m-1} & \text{for } \overset{(\alpha)}{\tau} \geqq \overset{(\alpha)}{\tau}_c, \qquad (11.1) \\[2ex] 0, & \text{for } \overset{(\alpha)}{\tau} < \overset{(\alpha)}{\tau}_c. \qquad (11.2) \end{cases}$$

Here m is the rate sensitivity parameter, $\overset{(\alpha)}{\dot{\gamma}}_0$ is a reference shear strain rate such that if the crystal is deformed with each $\overset{(\alpha)}{\dot{\gamma}}{}^p$ set equal to $\overset{(\alpha)}{\dot{\gamma}}_0$, then $\overset{(\alpha)}{\tau} = \overset{(\alpha)}{\tau}_c$, the critical resolved shear stress on the α^{th} slip system required to cause plastic deformation on that system (Pan and Rice [11]). A simple combined isotropic-kinematic hardening expression for $\overset{(\alpha)}{\tau}_c$ proposed by Weng [12], [16] is modified as follows

$$\overset{(\alpha)}{\tau}_c = \left\{ \tau_0 + \sum_\beta h[g + (1-g)\cos \overset{(\alpha\beta)}{\psi} \cos \overset{(\alpha\beta)}{\phi}] (\overset{(\beta)}{\gamma}{}^p)^n \right\} (1 - \nu\theta) \tag{12}$$

to account for the thermal softening effect. In Eq. (12), $\overset{(\alpha\beta)}{\psi}$ is the angle between the slip directions of the α^{th} and β^{th} slip systems, $\overset{(\alpha\beta)}{\phi}$ the angle between their slip normals, $\overset{(\beta)}{\gamma}{}^p$ the plastic strain of the β^{th} slip system, h the strength coefficient, n the work-hardening exponent, g the degree of anisotropy in work hardening, υ the coefficient of thermal softening, and the summation index β ranges over all slip systems. We note that $g = 1$ corresponds to Taylor's [13] isotropic hardening, and $g = 0$ to kinematic hardening. We refer the reader to Weng [12], [16] for details of the development of the isotropic-kinematic hardening model. That the thermal softening of a material can be modeled by an affine function of temperature has been pointed out by Bell [14] and Lin and Wagoner [15] based on their experimental observations. Whereas Bell has tested single crystals and polycrystalline materials, Lin and Wagoner based their conclusion upon tests conducted on a steel.

The resolved shear stress $\overset{(\alpha)}{\tau}$ of the α^{th} slip system is taken to be related to the local Cauchy stress σ_{ij} by

$$\overset{(\alpha)}{\tau} = \overset{(\alpha)}{v}_{ij}\sigma_{ij}, \tag{13}$$

where the Schmid factor $\overset{(\alpha)}{v}_{ij}$ is given by Eq. (8.1). The Cauchy stress rate corotational with the elastic distortion of the single crystal is assumed to be related to the elastic part of the strain-rate tensor through Hooke's law:

$$\overset{\nabla e}{\sigma}_{ij} = \left(K - \frac{2}{3}\,G\right) D^e_{kk}\delta_{ij} + 2GD^e_{ij}, \tag{14.1}$$

$$\overset{\nabla e}{\sigma}_{ij} = \dot{\sigma}_{ij} + \sigma_{ik}W^e_{kj} - W^e_{ik}\sigma_{kj}. \tag{14.2}$$

K and G equal, respectively, the bulk and shear moduli of the crystal whose elastic response has been assumed to be isotropic for the sake of simplicity. This assumption though unrealistic for single crystals has been employed by other investigators, e.g., see Weng [16]. Recalling that the Jaumann stress rate $\overset{\nabla}{\sigma}_{ij}$ corotational with the material element is given by

$$\overset{\nabla}{\sigma}_{ij} = \dot{\sigma}_{ij} + \sigma_{ik}W_{kj} - W_{ik}\sigma_{kj}, \tag{15}$$

we obtain

$$\overset{\nabla}{\sigma}_{ij} = \left(K - \frac{2}{3}\,G\right) D^e_{kk}\delta_{ij} + 2GD^e_{ij} + \sigma_{ik}W^p_{kj} - W^p_{ik}\sigma_{kj}. \tag{16}$$

For the boundary conditions we assume that all bounding surfaces are thermally insulated, the left and right vertical surfaces are traction free, the top and bottom surfaces are free of the tangential traction and on them a vertical component of velocity v_2 given by

$$v_2(t) = \begin{cases} \pm(t/t_r)\, v_0 & \text{for } \; 0 \leqq t \leqq t_r, \\ 1 & \text{for } \; t > t_r, \end{cases} \tag{17}$$

is prescribed. For the initial conditions we take

$$\varrho(\boldsymbol{x}, 0) = \varrho_0, \quad \boldsymbol{v}(\boldsymbol{x}, 0) = \boldsymbol{0}, \quad \boldsymbol{\sigma}(\boldsymbol{x}, 0) = \boldsymbol{0}, \quad \phi(\boldsymbol{x}, 0) = 0, \tag{18.1}$$

$$\theta(\boldsymbol{x}, 0) = \begin{cases} \varepsilon(1 - r^2)^9 \exp(-5r^2) & \text{for } \; r \leqq 1, \\ 0 & \text{for } \; r > 1, \end{cases} \tag{18.2}$$

where $r^2 = (X_1{}^2 + X_2{}^2)/H^2$, $2H$ being the length of a side of the square cross-section of the body. For $\varepsilon > 0$, the initial nonuniform temperature field represents a possible imperfection in the single crystal, and serves as a triggering mechanism for the localization of the deformation.

3 Numerical solution and results

We seek an approximate solution of the aforestated highly nonlinear problem by the finite element method. At each node, the mass density, two components of the velocity, temperature, four components σ_{11}, σ_{12}, σ_{22}, and σ_{33} of the Cauchy stress, and the angle ϕ characterizing the rotation of the slip system are taken as unknowns. The coordinates of nodes are updated after each time increment. The coupled nonlinear ordinary differential equations (ODEs) obtained by the Galerkin approximation of the field equations are integrated by using the backward-difference Adams method included in the subroutine LSODE taken from the package ODEPACK developed by Hindmarsh [17], and we set ATOL = RTOL = 10^{-3}. The subroutine adjusts the time step and the integration order in the Adams method adaptively until a solution of the coupled nonlinear ODEs has been computed to the desired accuracy. From the computed solution we evaluated $\overset{(\alpha)}{\tau}$, $\overset{(\alpha)}{\dot{\gamma}^p}$, D_{ij}^p, and W_{ij}^p at each quadrature point, and determined the plastic slip strain of each active slip system by using

$$\overset{(\alpha)}{\gamma^p}(t + \Delta t) = \overset{(\alpha)}{\gamma^p} + \Delta t[\overset{(\alpha)}{\dot{\gamma}^p}(t) + \overset{(\alpha)}{\dot{\gamma}^p}(t + \Delta t)]/2. \tag{19}$$

Even though LSODE allows up to 12th-order accurate integration method to be used, for the present problem, the highest order method used was only two and the maximum time step was found to be of the order of 10^{-3} µs. Thus, the error in the computations of slip strains should be of the same order as that in the computations of nodal values of the temperature and σ_{11}, etc. An alternative approach will be to regard Eq. (11.1) and (11.2) as field equations, obtain their weak forms by using the Galerkin method [18], and compute $\overset{(\alpha)}{\gamma^p}$ at each node point. This will increase the number of unknowns by a factor of 2.3 and thus require significantly more computational resources.

We modified Batra and Liu's [19] code to analyze the present problem and assigned following values to various material and geometric parameters.

$$\begin{aligned}
&k = 237\ \mathrm{Wm^{-1}\,{}^\circ C^{-1}}, \quad c = 960\ \mathrm{J\,kg^{-1}\,{}^\circ C^{-1}}, \quad \varrho_0 = 2\,700\ \mathrm{kg\,m^{-3}},\\
&G = 27.6\ \mathrm{GPa}, \quad K = 81.48\ \mathrm{GPa}, \quad \tau_0 = 55\ \mathrm{MPa}, \quad n = 0.52,\\
&h = 11.02\ \mathrm{MPa}, \quad m = 0.02, \quad \nu = 0.0222\,{}^\circ\mathrm{C}^{-1}, \quad H = 5\ \mathrm{mm},\\
&g = 0.28, \quad v_0 = 5\ \mathrm{ms^{-1}}, \quad t_r = 2\ \mu\mathrm{s}.
\end{aligned} \tag{20}$$

Thus, the average applied strain-rate equals $1\,000\ \mathrm{s}^{-1}$. Values of material parameters listed in (20) are representative for a single crystal of aluminium, except that a large value of the thermal softening coefficient ν is used to reduce the CPU time required for the initiation and development of the shear band. It should not affect the qualitative nature of results reported herein. Values of some of the material parameters are taken from Weng [16]. The low value 0.28 of g may imply that our assumption of all of the plastic working being converted into heating should be modified. However, such a modification will not affect the qualitative nature of results reported herein.

Results presented below are in terms of nondimensional variables obtained by scaling stress like quantities by τ_0, mass density by ϱ_0, length by H, time by H/v_0 and the temperature by θ_r where

$$\theta_r = \tau_0/\varrho_0 c = 21.2\,{}^\circ\mathrm{C}. \tag{21}$$

As a measure of the deformation at a point we use the maximum principal logarithmic strain defined by

$$\varepsilon_p = \ln \lambda_1 \simeq -\ln \lambda_2 \tag{22}$$

where $\lambda_1{}^2$, $\lambda_2{}^2$, and 1 are eigenvalues of the right Cauchy-Green tensor $C_{\alpha\beta} = x_{i,\alpha}x_{i,\beta}$, or the left Cauchy-Green tensor $B_{ij} = x_{i,\alpha}x_{j,\alpha}$, X_α being the coordinates of a material point in the stress-free undeformed configuration. The second relation in Eq. (22) holds because plastic deformations of the crystal are isochoric, and within the band elastic deformations are negligible.

The initial finite element mesh consisted of 32×32 uniform square elements, and we used 2×2 Gaussian quadrature rule to integrate various quantities over an element.

3.1 Results for no material imperfection

We first investigate the development of a shear band due to the heterogeneity of deformations caused by significantly varying contributions to the overall plastic deformations of the crystal from different slip systems. We examine two loadings, namely when the crystal is pulled and when it is compressed at an average strain-rate of $1000\ s^{-1}$. In each case, the initial temperature is assumed to be uniform.

3.1.1 Tensile loading along the crystallographic direction [380]

A study of the evolution of the accumulated plastic slip strains on different slip systems indicated that the slip systems $(111)[\bar{1}10]$, $(11\bar{1})[\bar{1}10]$, $(\bar{1}11)[110]$ and $(\bar{1}1\bar{1})[110]$ contributed equally and significantly to the plastic deformations of the single crystal. The plastic deformation on these slip systems first ensued at the top right and bottom left corners possibly because of the singularity of the deformations there since the boundary surfaces meeting there have different types of boundary conditions prescribed on them. This plastic deformation propagated into the body, and gradually concentrated into two narrow parallel regions at an angle of approximately 60° with the horizontal axis. Figure 1 shows contours of the accumulated plastic strain on one of these four slip systems at nondimensional time $t = 0.0575$. Note that the nondimensional time also equals the average strain. During subsequent deformations of the block, most of the deformations occurred within the two parallel narrow regions. The slip systems $(111)[01\bar{1}]$, $(11\bar{1})[011]$, $(\bar{1}11)[101]$ and $(1\bar{1}1)[\bar{1}01]$ also contributed to the plastic deformation of the body, the severely deformed regions of these slip systems were wider and were aligned along lines almost perpendicular to the centerlines of the narrow regions in which intense plastic deformations of the previous four slip systems were concentrated. Throughout the loading history studied herein, the plastic deformation everywhere in the body stayed minuscule (negligible for all practical purposes) on the remaining four slip systems, viz., $(111)[01\bar{1}]$, $(\bar{1}\bar{1}1)[101]$, $(\bar{1}11)[10\bar{1}]$, and $(\bar{1}1\bar{1})[011]$.

The value of the maximum plastic strain within the aforestated sets of severely deforming regions were essentially the same and it equalled 0.45 at nondimensional time $t = 0.0975$.

Figure 2 depicts contours of the angle ϕ of rotation of the crysal lattice at nondimensional time $t = 0.0975$. It is clear that the crystal lattice undergoes significant rotations in severely deformed regions where the two sets of aforestated slip systems are active, and at nondimensional time $t = 0.0975$ the maximum value of ϕ in each region equals 16.4° but the directions of rotation are opposite of each other. Contours of slip strain-rates on different slip systems resemble those of slip strains exhibited in Fig. 1, and are, therefore, not included herein.

The contours of the second invariant I of the nondimensional deviatoric strain-rate tensor $\tilde{D}_{ij}$ defined as

$$2I^2 = \tilde{D}_{ij}\tilde{D}_{ij}, \qquad \tilde{D}_{ij} = D_{ij} - \frac{1}{3} D_{kk}\delta_{ij}$$

are exhibited in Fig. 3 for an average strain (γ_{avg}) of 0.0975. The average strain is defined as the product of the nominal strain-rate and the elapsed time, and also equals the nondimensional

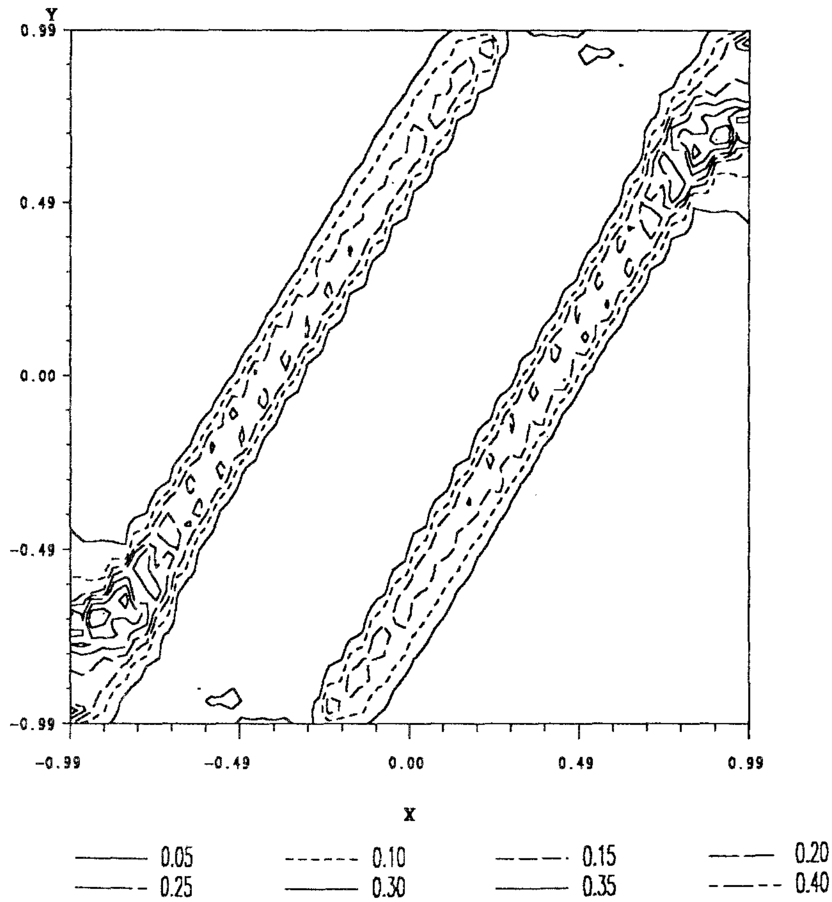

Fig 1. Contours of slip strains on any one of the four slip systems $(111)[\bar{1}10]$, $(11\bar{1})[\bar{1}10]$, $(\bar{1}11)[110]$, and $(\bar{1}1\bar{1})[110]$ at an average strain of 0.0575

time. The contours of the second invariant I_p of the nondimensional plastic strain-rate tensor D^p_{ij} look similar except that the magnitudes are different and are omitted for the sake of brevity. The values of D^p_{ij} are derived from the plastic straining of the slip systems, i.e., by using Eq. (7.1), those of D_{ij} are obtained from the spatial gradients of the global velocity field, i.e., by using Eq. (4). At an average strain of 0.0775, the maximum values of I and I_p, normalized by the nominal strain-rate of $1\,000\ \mathrm{s}^{-1}$, which need not occur at the same material point equal 13.7 and 17.8, respectively, suggesting that the micromechanisms of slip deformations of active slip systems are being delineated reasonably well. The minimum value zero of I_p indicates that at $\gamma_{\mathrm{avg}} = 0.0775$, some regions of the body are deforming elastically. At an average strain of 0.1, the maximum values of I_p and I equal 2206 and 12, respectively. Thus, the plastic straining of active slip systems becomes quite intense even though macrorate of deformation remains unchanged. The extent to which the coarseness of the finite element mesh contributes to the difference in the values of I and I_p has not been determined. Other reasons for the differences in the values of I and I_p are:

(i) values of $\boldsymbol{D}^p$ are computed from the data at Gauss points and involve no differentiation but those of $\boldsymbol{D}$ involve differentiation of the velocity field derived from nodal values of the velocity field and thus are less accurate than the values of $\boldsymbol{D}^p$;

(ii) $D_{33} = 0$ because of the assumption of plane strain but D^p_{33} need not equal 0;

(iii) because of the rather small value of m, a 10% change in the value of τ_c can change the value of $\dot{\gamma}^p$ by a factor of 100;

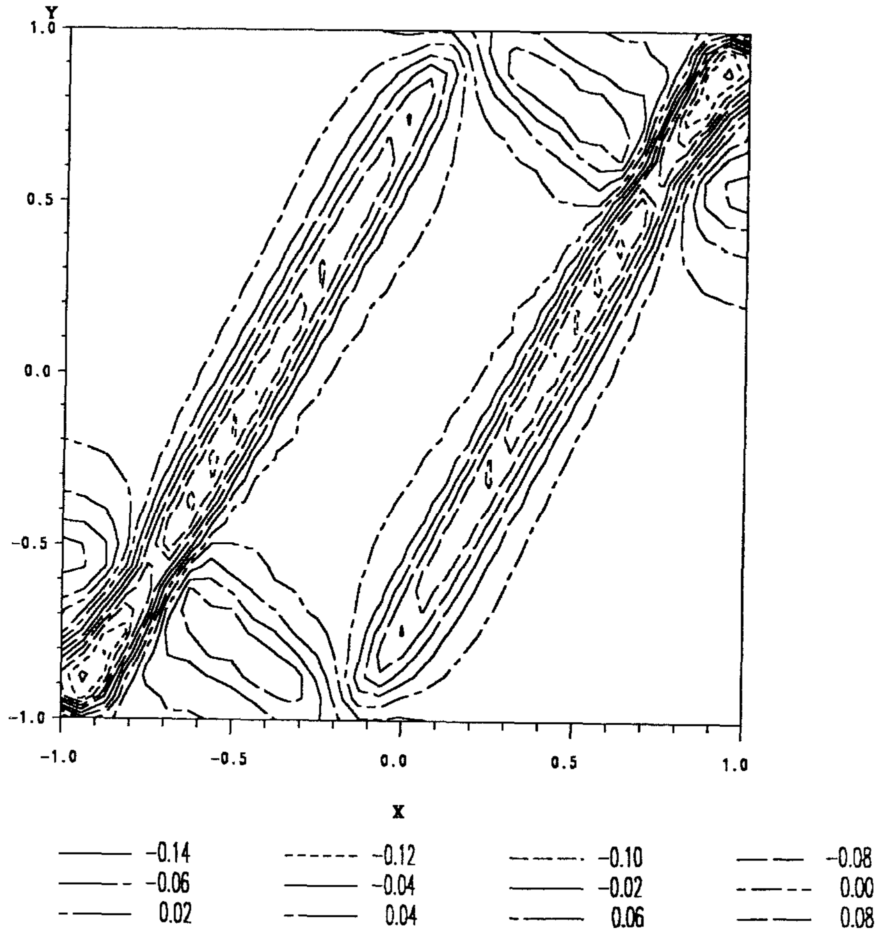

Fig. 2. Contours of the angle of rotation of the crystal lattice at an average strain of 0.0575

(iv) stress waves may have not been completely attenuated and thus may affect the instantaneous values of I and I_p; and

(v) rotations of the slip systems and the temperature rise at a Gauss point can easily change the value of τ_c by 10%.

The reason for computing $\boldsymbol{D}^p$ and $\boldsymbol{D}$ from data at different points is given after Eq. (19).

The contours of the maximum principal logarithmic strain ε_p and the temperature rise at an average strain of 0.0975 look similar to those of I_p depicted in Fig. 3. The maximum and minimum values of ε_p at any point within the body and at $t = 0.0975$ equal 0.58 and 0.016, respectively, and the maximum value of ε_p was found to be higher than the maximum value of the slip strain on any one of the 12 slip systems. A reason for the maximum value of ε_p being greater than the maximum value of slip strains is that within a small region all slip systems are active simultaneously. The peak temperature rise equals 33 °C but because of the rather large value of the coefficient of thermal softening assumed in our work, the value of the critical shear stress is reduced to 26.6% of its value when the term $(1 - \nu\theta)$ is omitted in the expression (12) for the critical shear stress. Thus, softening of the material because of its being heated up facilitates its further plastic deformation.

The deformed mesh at an average strain of 0.0975 shown in Fig. 4 reinforces what can be concluded from the contours of slip strains, the angle of rotation and the second invariant of the deviatoric strain-rate tensor exhibited in Figs. 1, 2, and 3, respectively, that the intense

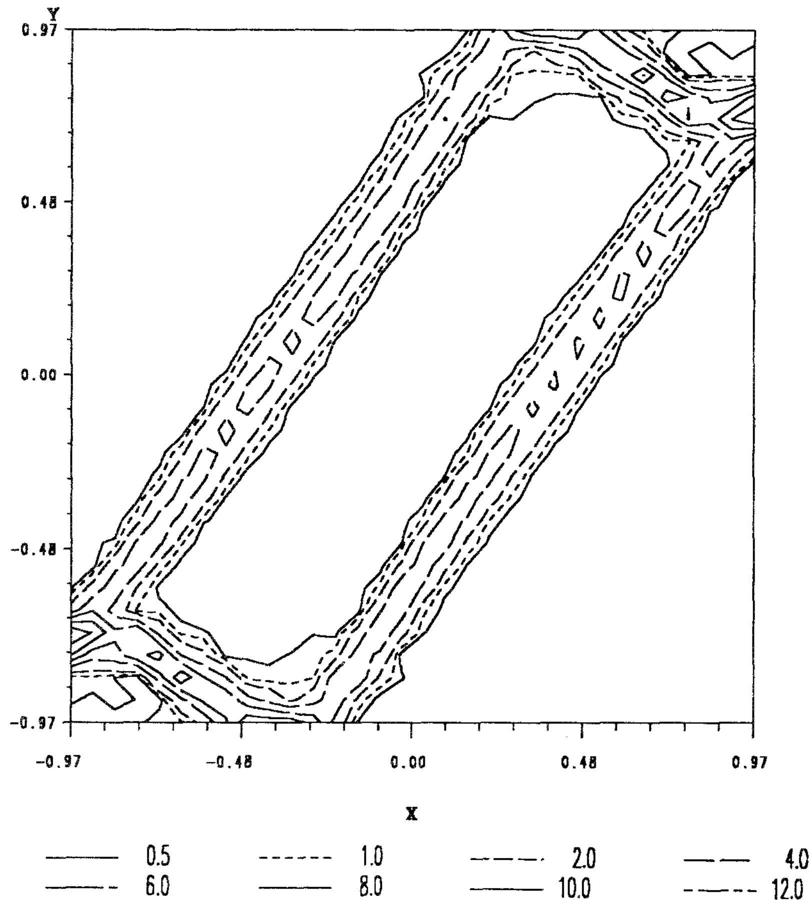

Fig. 3. Contours of the second invariant of the non-dimensional deviatoric strain-rate tensor at an average strain of 0.0975

deformations of the body are concentrated along the sides of a parallelogram. The plot of the vertical component of the velocity, not shown due to the limitations of space, indicates that at an average strain of 0.0975, the body is divided into several regions each moving as a rigid body and the vertical component of velocity changes sharply across the boundaries of these regions.

3.1.2 Compressive loading along the crystallographic direction [380]

As in the previous case, two sets of slip systems, namely $(111)[\bar{1}10]$, $(11\bar{1})[\bar{1}10]$, $(\bar{1}11)[110]$, $(\bar{1}1\bar{1})[110]$, and $(111)[01\bar{1}]$, $(11\bar{1})[011]$, $(\bar{1}11)[101]$, $(1\bar{1}1)[\bar{1}01]$ are quite active and contribute significantly to the plastic deformations of the body. The contours of slip strains of one slip system from the first set at an average strain, γ_{avg}, of 0.0575 are exhibited in Fig. 5. Whereas the slip strains on the first set of slip systems contribute to the plastic deformation of the region near the top right and bottom left corners, that on the second set of slip systems deform noticeably the central longitudinal region. At an average strain, γ_{avg}, of 0.0975, the maximum value of slip strain in the first and second sets of slip systems equals 1.076 and 0.381, respectively. The other four slip systems, i.e., $(111)[\bar{1}01]$, $(\bar{1}\bar{1}1)[101]$, $(\bar{1}11)[01\bar{1}]$, and $(\bar{1}1\bar{1})[011]$ stay dormant until the average axial strain reaches 0.0575 at which instant they start making a contribution to the plastic deformations of a very small region near the top right and bottom left corners. At $\gamma_{avg} = 0.0575$, 0.0775, and 0.0975, the maximum values of the slip strain on a slip system from this set equal

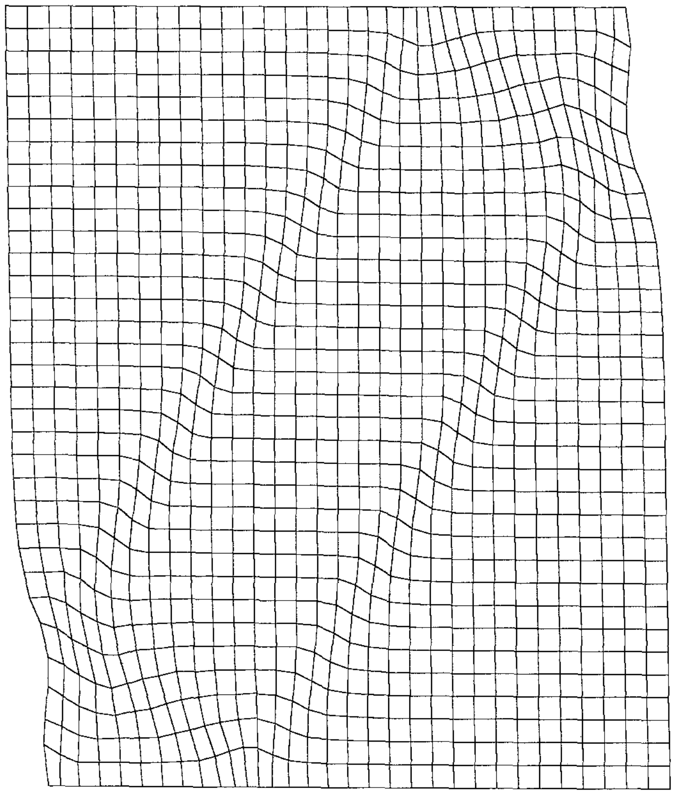

Fig. 4. Deformed mesh at an average strain of 0.0975

0.048, 0.235, and 0.417, respectively. However, the region over which these slip systems are active is quite small. One reason for these slip systems to begin contributing towards the plastic deformation of the body at $\gamma_{avg} = 0.0575$ is the noticeable rotation of the lattice structure during its plastic deformation; Fig. 6 depicts the contours of the angle of rotation ϕ at $\gamma_{avg} = 0.0575$. The maximum values of ϕ in the severely deformed regions near the top right and bottom left corners and in the central longitudinal region equal 25.5° counterclockwise and 15.8° clockwise, respectively.

We note that the regions in which the first two sets of slip systems are active are quite different when the crystal is loaded in tension and compression. At an average strain of 0.0975 the maximum value of slip strain on any slip system equalled 1.076 and 0.486 for compression and tension loading, respectively. One reason for this difference is that the region deformed more severely is smaller when the body is compressed as compared to that when it is pulled.

From the computed results, we evaluated the nondimensional second invariant I of the deviatoric strain-rate tensor $\boldsymbol{D}$ and the nondimensional second invariant I_p of the plastic strain-rate tensor $\boldsymbol{D}^p$. The maximum values of I and I_p at average strains of 0.0075, 0.02775, 0.0375, 0.0475, 0.0575, 0.0775, and 0.0975 equal (3.62, 7.13), (7.44, 9.09), (13.47, 32.28), (23.20, 45.13), (18.99, 60.15), (17.84, 856), and (19.22, 7457), respectively. Note that the maximum values of I and I_p need not occur at the same material point. When the average strain exceeds 5%, the region in which slip systems are active and contribute to the plastic deformation of the body narrows down measurably, and the slip strain-rate there increases significantly to accommodate the imposed nondimensional average strain-rate of 1. However, the region in which I has nonzero values is still large as compared to that in which $I_p > 0$, therefore, the peak value of

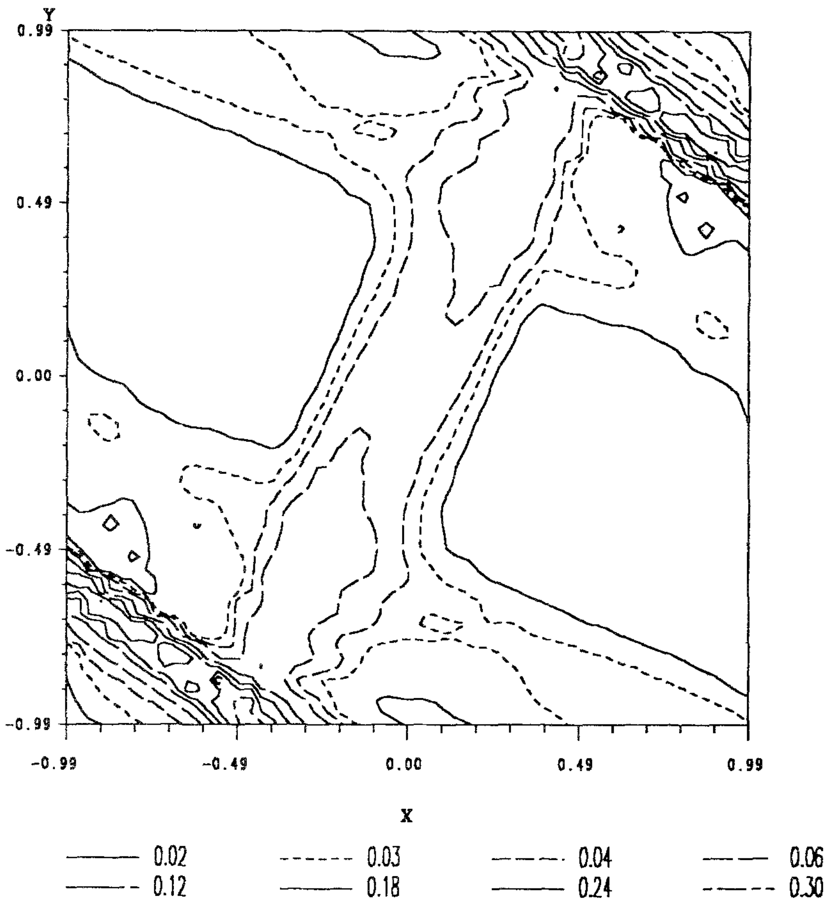

Fig. 5. Contours of slip strains on any one of the four slip systems $(111)[\bar{1}10]$, $(11\bar{1})[\bar{1}10]$, $(\bar{1}11)[110]$, and $(\bar{1}1\bar{1})[110]$ at an average strain of 0.0575

I does not increase as rapidly as the peak value of I_p does. Other plausible reasons for the differences in the values of I and I_p are enumerated in the previous section.

Figure 7 depicts contours of the maximum principal logarithmic strain ε_p at an average strain of 0.0975. The maximum value 1.158 of ε_p suggests that deformations within the band are more intense than those in the previous case when the single crystal was pulled so as to induce the same average tensile strain. At the hottest point within the band, the thermal softening effect reduces the critical shear stress to 11.94% of its value in the absence of thermal softening. From the contours of the maximum principal logarithmic strain, one can see that the shear band is in the form of the letter Z turned upside down rather than a parallelogram obtained in the previous case.

3.2 Material imperfection modelled by nonuniform initial temperature

We assume that the initial temperature is given by Eq. (18.2) with $\varepsilon = 1.0$, and the single crystal is compressed along the crystallographic direction [380]. The maximum value of the initial temperature perturbation is intentionally taken to be large so as to reduce the computational time. It will facilitate the comparison of presently computed results with those of Zhu and Batra [6] who used a different loading configuration for the FCC single crystal. Because of the initial higher temperature at the center, the material there is softer and easy to deform. Contours of slip strains

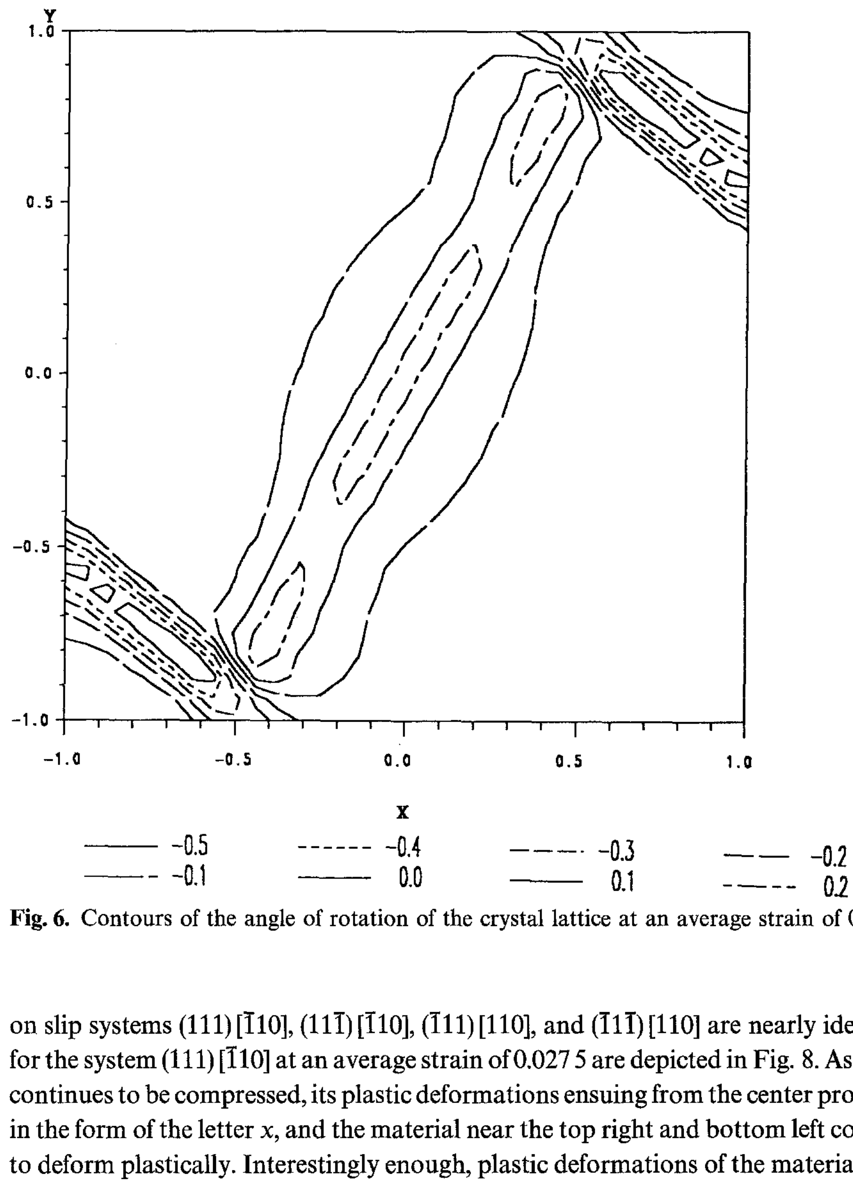

Fig. 6. Contours of the angle of rotation of the crystal lattice at an average strain of 0.0575

on slip systems $(111)[\bar{1}10]$, $(11\bar{1})[\bar{1}10]$, $(\bar{1}11)[110]$, and $(\bar{1}1\bar{1})[110]$ are nearly identical, and those for the system $(111)[\bar{1}10]$ at an average strain of 0.0275 are depicted in Fig. 8. As the single crystal continues to be compressed, its plastic deformations ensuing from the center propagate outwards in the form of the letter x, and the material near the top right and bottom left corners also begins to deform plastically. Interestingly enough, plastic deformations of the material in these regions recede rather than intensify with the passage of time, and eventually intense plastic deformations of the material along the line making an angle of 34° clockwise with the horizontal persist. It is because in compression the 34° direction is more favorable to plastic deformation than the one perpendicular to it. Contours of slip strains on any one of the slip systems $(111)[01\bar{1}]$, $(111)[01\bar{1}]$, $(\bar{1}11)[101]$ and $(1\bar{1}1)[\bar{1}01]$ are almost identical to each other and are omitted to conserve space. The material region wherein these slip systems are active looks like a star and the plastic deformation therein continues to intensify and propagate outwards with an increase in the overall deformations of the crystal. No measurable or detectable plastic deformation occurs on the other four slip systems, viz. $(111)[\bar{1}01]$, $(\bar{1}\bar{1}1)[101]$, $(\bar{1}11)[01\bar{1}]$, and $(\bar{1}1\bar{1})[011]$, until the average strain of 0.0275 at which instant these slip systems begin contributing to the plastic deformation of the body. Slip strains on these slip systems are essentially the same, and the narrow intensely deformed region is oriented at an angle of approximately 30° clockwise from the horizontal axis. The maximum values of the slip strain on the three sets of slip systems when $\gamma_{avg} = 0.0575$ equal 0.3986, 0.1209, and 0.3348, respectively. However, these need not occur at the same point.

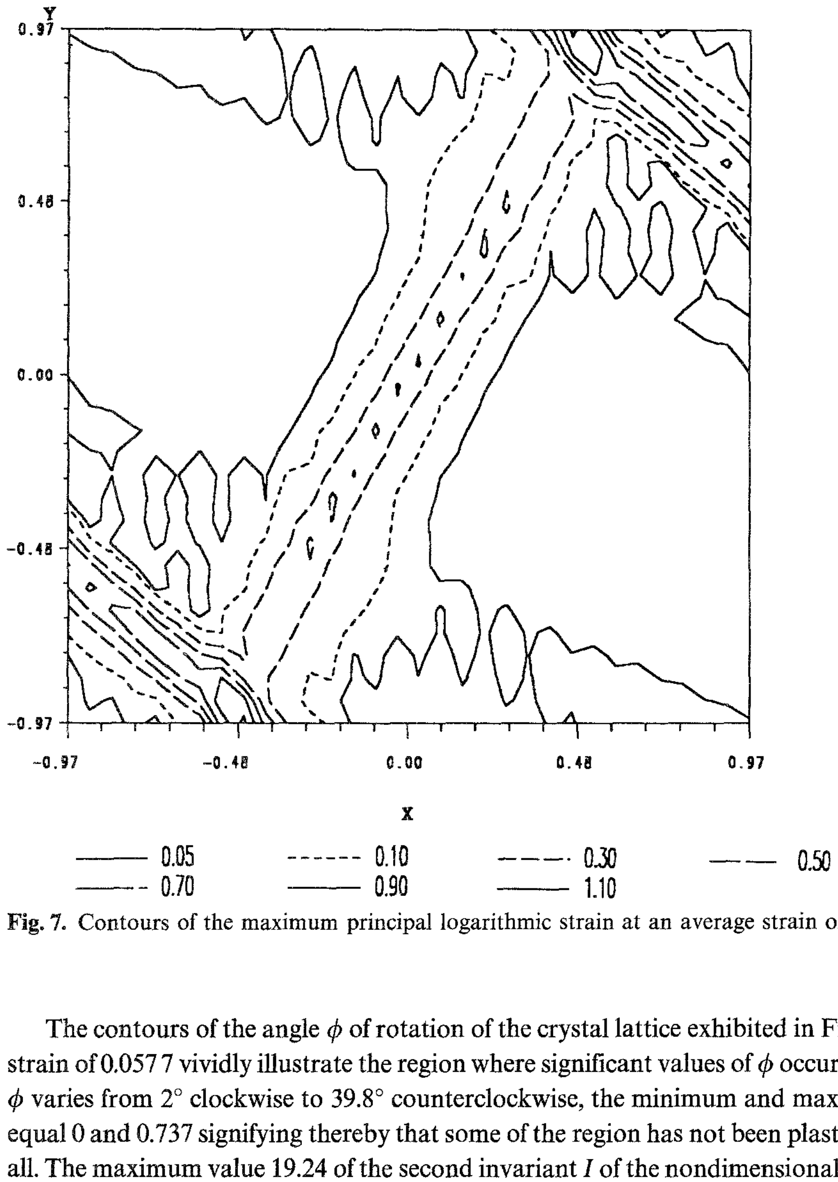

Fig. 7. Contours of the maximum principal logarithmic strain at an average strain of 0.0975

The contours of the angle ϕ of rotation of the crystal lattice exhibited in Fig. 9 at an average strain of 0.0577 vividly illustrate the region where significant values of ϕ occur. At $\gamma_{avg} = 0.0575$, ϕ varies from 2° clockwise to 39.8° counterclockwise, the minimum and maximum values of ε_p equal 0 and 0.737 signifying thereby that some of the region has not been plastically deformed at all. The maximum value 19.24 of the second invariant I of the nondimensional strain-rate tensor $\boldsymbol{D}$ indicates that peak strain-rates equal $1.9 \times 10^4\ s^{-1}$, and the peak nondimensional temperature of 1.97 implies that the critical shear stress at the point where the peak temperature occurs equals 7.2% of its value in the absence of the thermal softening effect. The deformed mesh at $\gamma_{avg} = 0.0575$ not shown herein illustrates that the shear band is inclined at an angle of nearly 30° clockwise with the horizontal and does not pass through a corner.

Zhu and Batra [6] recently studied the problem when the single crystal was compressed along the crystallographic direction [010] and plane of deformation was parallel to the plane (001) or $(10\bar{1})$. They assumed the deformations to be symmetric about the horizontal and vertical centroidal axes and analyzed deformations of the material in the first quadrant. When the plane of deformation was parallel to the plane (001) of the single crystal, a single shear band originated from the center of the cross-section, propagated along a line making an angle of 45° with the horizontal, and was reflected back from the top loading surface with the angle of reflection being essentially equal to the angle of incidence. For the case of the plane of deformation being parallel to the plane $(10\bar{1})$ of the single crystal, the shear band originating from the center of the

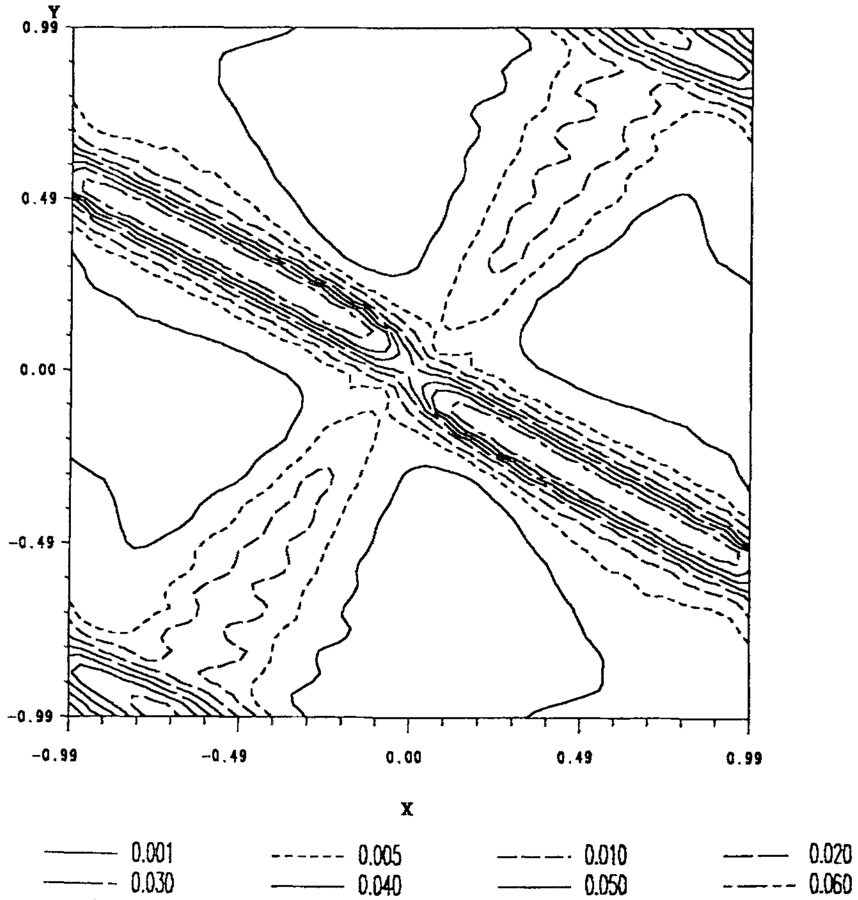

Fig. 8. Contours of slip strains on any one of the four slip systems (111) [$\bar{1}$10], (11$\bar{1}$) [$\bar{1}$10], ($\bar{1}$11) [110], and ($\bar{1}$1$\bar{1}$) [110] at an average strain of 0.027 5

cross-section propagated along the line making an angle of 39.5° with the horizontal, and eventually split into two parallel bands. Different slip systems were found to be active in each case.

3.3 Material imperfection modelled by a misorientation of the crystal lattice

We now assume that the initial temperature is uniform but four elements meeting at the centroid of the cross-section are misoriented by 10°. Thus the deformations of these four elements will be different from that of the rest of the body, and these elements may act as nuclei of shear bands or may not deform much. For the single crystal compressed along the crystallographic direction [380], the contours of the accumulated slip strains on any one of the four slip systems (111) [$\bar{1}$10], (11$\bar{1}$) [$\bar{1}$10], ($\bar{1}$11) [110], and ($\bar{1}$1$\bar{1}$) [110] at average strain, γ_{avg}, of 0.007 5, 0.047 5, 0.077 5 and 0.097 5 vividly demonstrate that intense plastic deformation on these slip systems initiates from the top right and bottom left corners and propagates inwards; the contours of the accumulated slip strains at an average strain of 0.007 5 are shown in Fig. 10. We note that these bands do not pass through the center. Since the slip systems within the central four elements are different from those outside of them, this region is found to be less amenable to severe plastic deformations and resists the propagation of shear bands through it. The contours of the accumulated slip strains on slip

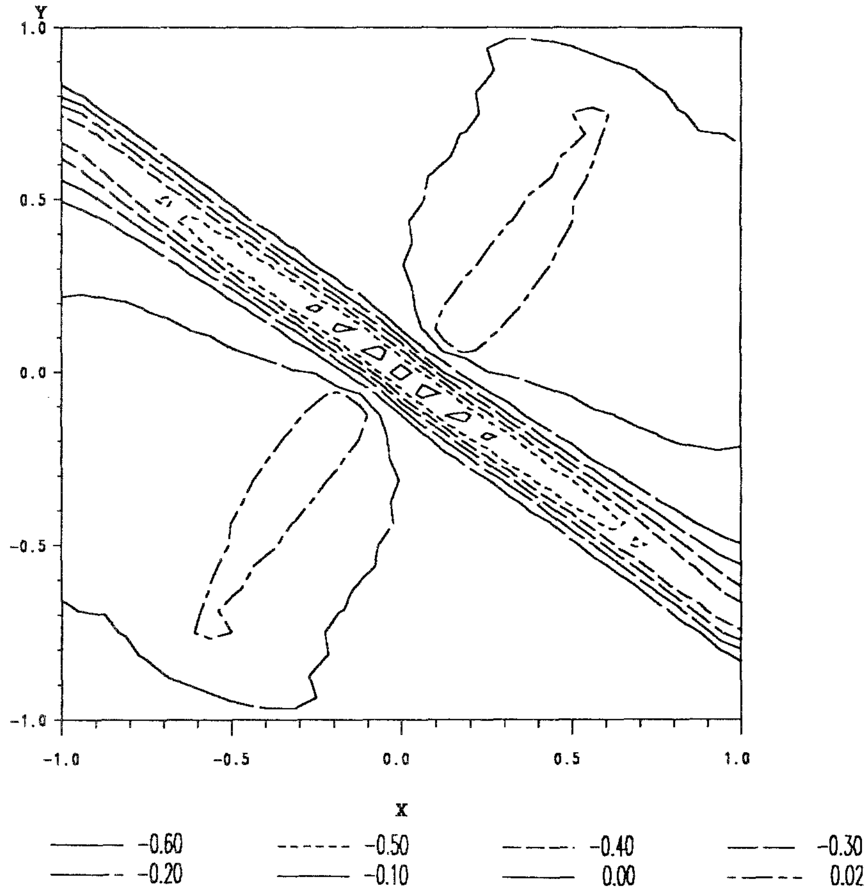

Fig. 9. Contours of the angle of rotation of the crystal lattice at an average strain of 0.0575

systems (111) [01$\bar{1}$], (11$\bar{1}$) [011], ($\bar{1}$11) [101], and ($\bar{1}$1$\bar{1}$) [011] at γ_{avg} = 0.0075, 0.0475, 0.0775 and 0.0975 reveal that severe plastic deformations on them occur near the boundaries of the central four elements and propagate outwards. The remaining four slip systems (111) [$\bar{1}$01], ($\bar{1}\bar{1}$1) [101], ($\bar{1}$11) [01$\bar{1}$] and ($\bar{1}$1$\bar{1}$) [011] stay inactive until the crystal has been compressed to an average strain of 0.057 at which point they become active in a very narrow region. At an average strain of 9.75%, the maximum value of the accumulated plastic strain on these three sets of slip systems equals 37.1%, 16.9%, and 17.4%, respectively. Contours of the angle of rotation ϕ of the crystal lattice at γ_{avg} = 0.0775 are plotted in Fig. 11. At an average strain of 0.0975, peak values of ϕ in the two severely deformed regions equal 9° clockwise and 25.4° counterclockwise.

The peak value 1.325 of the rise in nondimensional temperature lowers the critical shear stress by 62.4%, maximum and minimum values of nondimensional I equal 17.06 and 0.0087, and ε_p takes on values between 0 and 0.51. Thus there is at least one material point in the body that has not been deformed plastically at all. The deformed mesh at an average strain of 0.1275 reveals that severe deformations of the body occur along two parallel lines on either side of the centroid and making an angle of about 35° counterclockwise with the horizontal. The intensely deformed region essentially coincides with the one wherein large rotations of the crystal lattice occur.

Figure 12 depicts the time-history of the magnitude of the average axial stress acting on the top surface for the four cases considered above. We note that the body is pulled in the first case

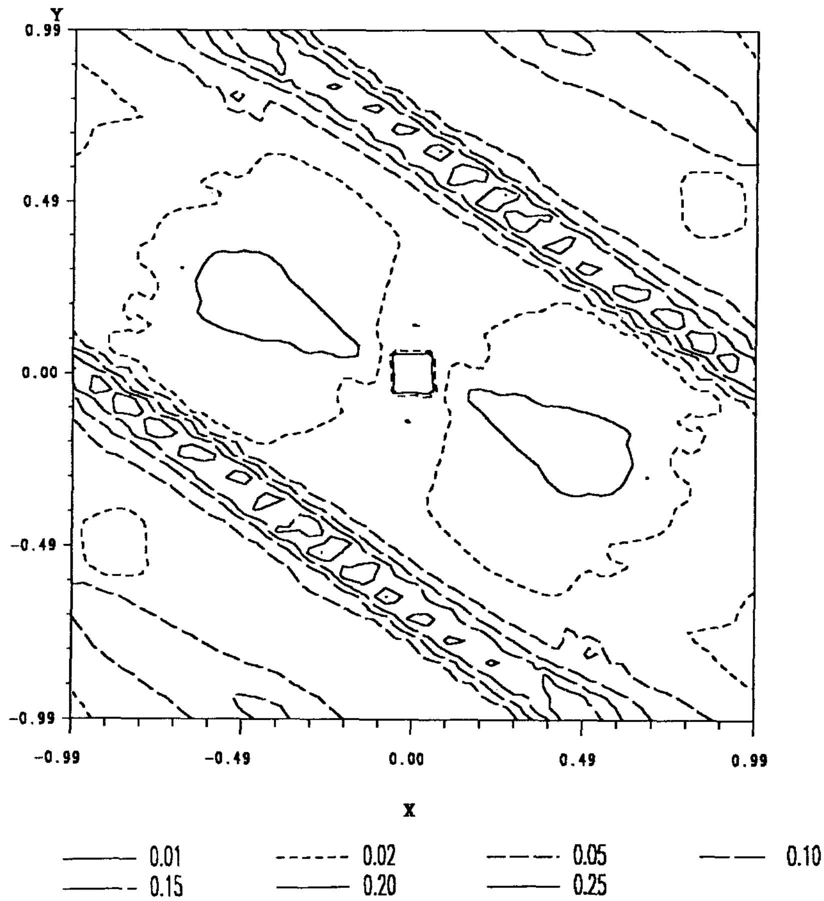

Fig. 10. Contours of slip strains on any one of the four slip systems (111) [$\bar{1}$10], (11$\bar{1}$) [$\bar{1}$10], ($\bar{1}$11) [110], and ($\bar{1}$1$\bar{1}$) [110] at an average strain of 0.0775

but is compressed in the remaining three cases. A comparison of curves A and B suggests that there is no major difference in the overall response of the crystal to the prescribed deformation rate. In each one of the four cases studied, the stress magnitude drops at a rather low value of the average strain; the stress drop is more rapid for the case of temperature perturbation. It is due to the rather high values of the initial temperature assumed at the centroid of the body, and also of the thermal softening coefficient. The oscillations in the curve C signify that stress waves have not been attenuated completely whereas those for the other three cases have been. A comparison of curves A, B, and D reveals that the misorientation by 10° of a small region near the block centroid does not affect in any noticeable way the overall response of the crystal. However, the shapes and locations of the shear bands formed in each case are different.

4 Conclusions

We have studied dynamic plane strain thermomechanical deformations of a FCC single crystal loaded along the crystallographic direction [380] with the plane of deformation being parallel to the plane (001) of the crystal. The prismatic body has square cross-section with all boundaries thermally insulated, the two vertical surfaces traction free, the two horizontal surfaces are free of tangential tractions but a normal velocity is prescribed on them so as to induce an average

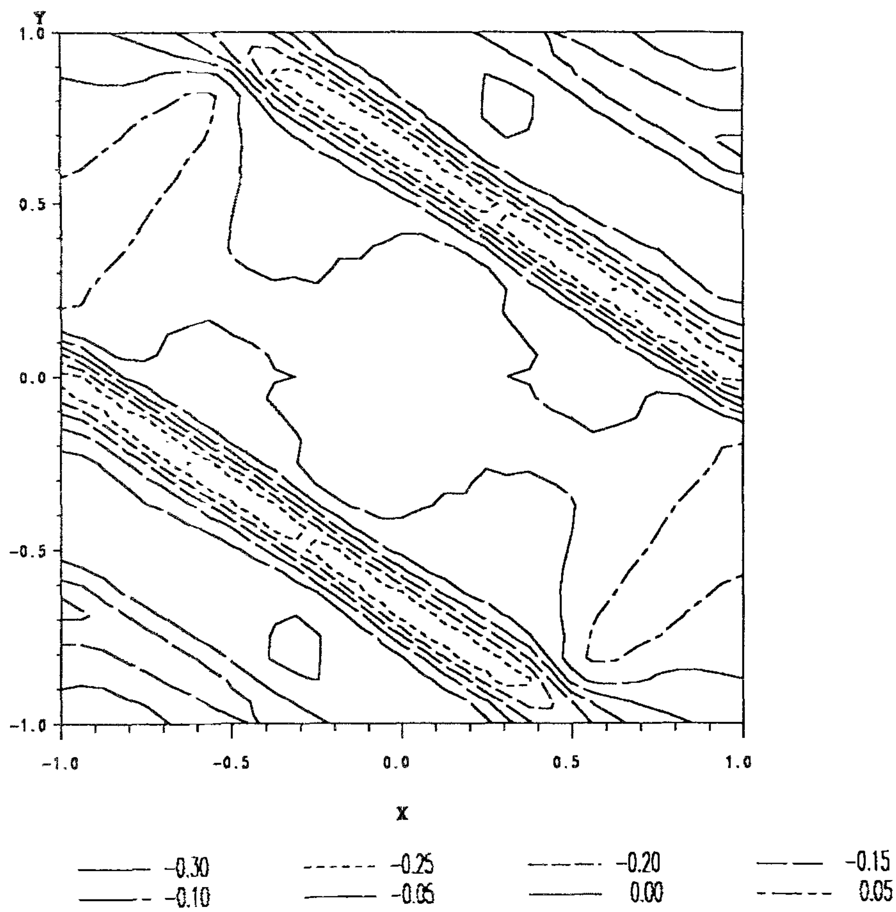

Fig. 11. Contours of the angle of rotation of the crystal lattice at an average strain of 0.0775

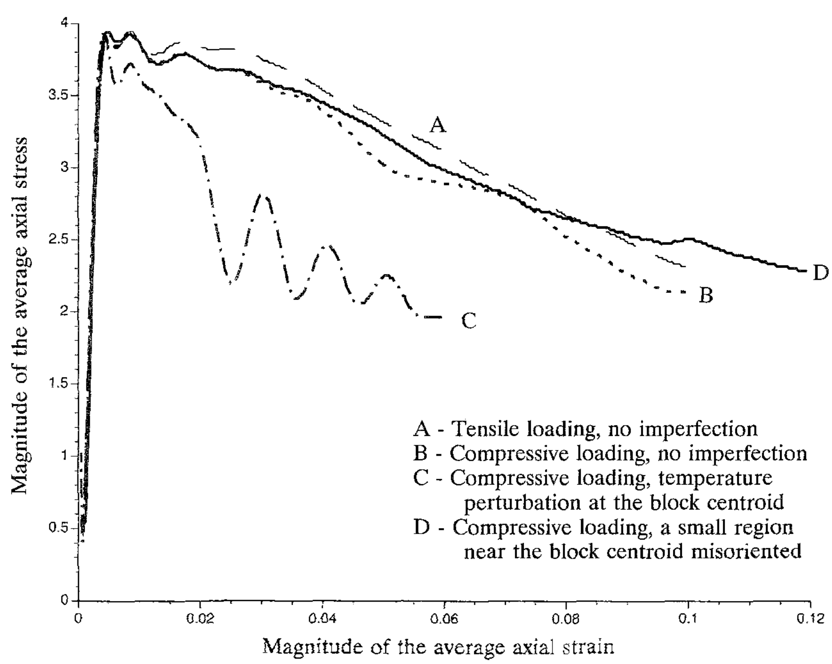

Fig. 12. Magnitude of the average normal stress vs. magnitude of the average normal strain for the four cases studied

normal strain-rate of $1\,000\ s^{-1}$. In the first set of computations there is no material imperfection presumed, and the body is either pulled or compressed. In the second set of problems, the body is assumed to have an imperfection either in the form of an initial nonuniform temperature with the maximum temperature at its centroid or a small region around the centroid is misoriented and the body is loaded in compression. In each case all twelve slip systems are assumed to contribute to the plastic deformations of the body.

In each one of the four cases studied, the two sets of four slip systems, viz., $(111)[\bar{1}10]$, $(11\bar{1})[\bar{1}10]$, $(\bar{1}11)[110]$, $(\bar{1}1\bar{1})[110]$, and $(111)[01\bar{1}]$, $(11\bar{1})[011]$, $(\bar{1}11)[101]$, $(1\bar{1}1)[\bar{1}01]$ became active in different regions soon after the body was loaded. The other four slip systems either stayed dormant throughout the loading process, or became active after the body had been deformed by a certain amount. When there is no imperfection introduced, the singularity of the deformations at the corners caused the shear bands to initiate there and propagate inwards into the body. The severely deformed region is in the form of a parallelogram when the body is pulled, and the letter Z turned upside down when compressed. For the case of the nonuniform initial temperature with the maximum temperature at the centroid of the cross-section, the shear band passed through the centroid and made an angle of approximately 34° counterclockwise with the horizontal. An initial misorientation of the lattice structure in a small region surrounding the centroid of the cross-section resulted in two parallel bands on either side of the centroid and inclined at an angle of about 35° counterclockwise with the horizontal.

Acknowledgements

This work was supported by the U.S. Army Research Office grant DAAL 03-91-G-0084 and the U.S. NSF grant CMS9411383 to the Virginia Polytechnic Institute and State University. Some of the computations were performed on the NSF sponsored supercomputer center in Ithaca, NY.

References

[1] Sawkill, J., Honeycombe, R. W. K.: Strain-hardening in face centered cubic metal crystals. Acta Metall. **2,** 854 (1954).

[2] Price, R. J., Kelly, A.: Deformation of age-hardened aluminium alloy crystals-II. fracture. Acta Metall. **12,** 319 (1964).

[3] Saimoto, S., Hosford, W. F., Backofen, W. A.: Ductile fracture in copper single crystals. Phil. Mag. **12,** 319 (1965).

[4] Chang, Y. W., Asaro, R. J.: An experimental study of shear-localization in aluminium-copper single crystals. Acta Metall. **29,** 241 (1981).

[5] Zikry, M. A., Nemat-Nasser, S.: High strain-rate localization and failure of crystalline materials. Mech. Mater. **10,** 215–237 (1990).

[6] Zhu, Z. G., Batra, R. C.: Analysis of dynamic shear bands in a FCC single crystal. Int. J. Plasticity **9,** 653–696 (1993).

[7] Koehler, J. S.: The nature of work-hardening. Phys. Rev. **86,** 52 (1952).

[8] Orowan, E.: Dislocation in metals. American Institute of Mining, Metallurgical and Petroleum Engineers, NY, p. 103 (1954).

[9] Farren, W. S., Taylor, G. I.: The heat developed during plastic extrusion of metal. Proc. R. Soc. London Ser. **A107,** 422 (1925).

[10] Sulijoadikusumo, A. U., Dillon, O. W., Jr.: Temperature distribution for steady axisymmetric extrusion, with an application to Ti-6Al-4V; Parts 1, 2, 3. J. Thermal Stresses **2,** 97 (1979).

[11] Pan, J., Rice, J. R.: Rate sensitivity of plastic flow and implication for yield surface vertices. Int. J. Solids Struct. **19,** 973–987 (1983).

[12] Weng, G. J.: Dislocation theories of work hardening and yield surfaces of single crystal. Acta Mech. **37**, 217–230 (1980).
[13] Taylor, G. I.: Plastic strain in metals. J. Inst. Metal. **62-1**, 307–324 (1938).
[14] Bell, J. F.: Physics of large deformations of crystalline solids. Berlin Heidelberg New York: Springer 1968.
[15] Lin, M. R., Waggoner, R. H.: Effect of temperature, strain, and strain-rate on the tensile flow stress of I.F. steel and stainless steel type 310. Scripta Metall. **20**, 143–148 (1986).
[16] Weng, G. J.: Kinematic hardening rule in single crystals. Int. J. Solids Struct. **15**, 861–870 (1979).
[17] Hindmarsh, A. C.: ODEPACK: A systematized collection of ODE solvers. In: Scientific computing (Stepleman, R. A., et al., eds.), pp. 55–64. Amsterdam: North-Holland 1983.
[18] Hughes, T. J. R.: The finite element method. Linear static and dynamic finite element analysis. Englewood Cliffs: Prentice-Hall 1987.
[19] Batra, R. C., Liu, D. S.: Adiabatic shear banding in plane strain problems. J. Appl. Mech. **56**, 527–534 (1989).

Authors' addresses: R. C. Batra, Department of Engineering Science and Mechanics, Virginia Polytechnic Institute and State University, Blacksburg, VA 24061-0219, U.S.A.; and Z. G. Zhu, 2465 Somerset, Apt. 206, Troy, MI, 48084, U.S.A.